



Cavitation level-acoustic intensity hysteresis: experimental and numerical characterization

Pauline Labelle, Claude Inserra, Jean-Christophe Béra

► To cite this version:

Pauline Labelle, Claude Inserra, Jean-Christophe Béra. Cavitation level-acoustic intensity hysteresis: experimental and numerical characterization. *Acoustics 2012*, Apr 2012, Nantes, France. <hal-00810730>

HAL Id: hal-00810730

<https://hal.science/hal-00810730v1>

Submitted on 23 Apr 2012

HAL is a multi-disciplinary open access archive for the deposit and dissemination of scientific research documents, whether they are published or not. The documents may come from teaching and research institutions in France or abroad, or from public or private research centers.

L'archive ouverte pluridisciplinaire **HAL**, est destinée au dépôt et à la diffusion de documents scientifiques de niveau recherche, publiés ou non, émanant des établissements d'enseignement et de recherche français ou étrangers, des laboratoires publics ou privés.



HAL Authorization



Cavitation level-acoustic intensity hysteresis: experimental and numerical characterization

P. Labelle^a, C. Inserra^b and J.-C. Béra^b

^aUniversité Lyon 1 / INSERM, LabTAU - U1032, 151 Cours A. Thomas, 69424 Lyon, France,
Metropolitan

^bApplication des ultrasons à la thérapie, Pôle santé Lyon est, 151 cours Albert Thomas 69424
Lyon cedex 03
pauline.labelle@inserm.fr

In therapeutic applications such as sonoporation, inertial cavitation is commonly considered as the main candidate inducing membrane poration. Thus, characterizing inertial cavitation, as related to bubble size distribution and medium history, is of great importance. When applying successive ultrasonic shots for increasing acoustic intensities, the inertial cavitation level sharply increases around the inertial cavitation threshold. The curve of the inertial cavitation level versus acoustic intensity is different when decreasing the acoustic intensity: the threshold obtained is lower. This effect, characterized by the area of the hysteresis loop, and attributed to the change in bubble size distribution, is studied experimentally and numerically. In our experiments, the hysteresis effect is observed on the inertial cavitation level but also on the amplitude of harmonics or ultra-harmonics of the fundamental frequency. Numerically, the main mechanisms responsible for this hysteresis were identified as rectified diffusion and fragmentation during acoustic excitation, and dissolution and rising bubbles when acoustic excitation is off. Starting from a given bubble size distribution, the change in bubble size distribution is obtained for increasing and decreasing acoustic intensity. The hysteresis of inertial cavitation (quantified by bubbles collapse energy) and its dependence on time off show qualitative agreement with experimental results.

1 Introduction

Acoustic cavitation is often the common denominator of a wide range of therapeutic applications using biomedical acoustics [1]. It consists of the nucleation of gas or vapour bubbles in a liquid, and of their oscillations under pressure waves. There are two kinds of cavitation activity: stable cavitation, which is the linear and non-linear radial oscillation of bubbles; and inertial cavitation, which is the violent collapse of bubbles [2]. This first kind of cavitation is characterized by the apparition of the sub-harmonic of the fundamental frequency in the spectrum and the second one by the elevation of the broadband noise. It is inertial cavitation which appears to play an important role in some therapeutic ultrasound applications as sonoporation [3,4]. In [5], the evolution of the inertial cavitation level versus acoustic intensity is very variable, and especially for medium acoustic intensities. Indeed for intensities lower than 0.2 and higher than 1.2 W/cm², the standard deviation of the inertial cavitation level is less important. This large surface of inertial cavitation level possibilities suggests a hysteresis effect between the inertial cavitation level and the acoustic intensity. In [6] a huge difference in acoustic spectra, for increasing and decreasing intensity, with regards to their history, has been observed. But their experimental observations did not allow to conclude on significant hysteresis effect. In this study, we focus on the hysteresis effect noticed on inertial cavitation. The observed hysteresis curve is studied experimentally before a numerical investigation by modelling the main mechanisms involved in this effect.

2 Experimental investigation

2.1 Experimental setup

A plane piezoelectric transducer (frequency 501 kHz, diameter 20 mm) is immersed in a degassed water bath (20 L tank, O₂ rate in water between 2.3 and 3.7 mg/L). The transducer is located such as its acoustic axis is vertical and covered by 14 mm of water above its surface (Figure 1). The transducer, electrically matched to 50 Ω , generates a continuous sinusoidal wave provided by a function generator (HP 33120 A), successively amplified by a variable gain amplifier (AD 603) and a power amplifier (50 dB, 200 W, Adece). The electrical power delivered by the generator is ranged between -12 and 9 dBm, which correspond to acoustic intensities between 0.1 and 12.8 W/cm².

The sonicated media is composed by 2 mL of degassed water at ambient temperature placed in a well of a culture plate in

polystyrene (12 wells, diameter 20 mm, BD sciences). The sonicated well is located above the transducer and its height is adjusted so that the liquid surface corresponds to a node of the stationary wave field of the irradiated medium.

A home-made hydrophone (cutting frequency 10 MHz) realized with a PVDF film (diameter 10 mm) molded in resin (AY 103, Araldite) is located in the vicinity of the transducer. It allows listening the cavitation noise in the exposed medium. The received signal is amplified (20 dB, NF Electronic Instrument® BX31), digitized (acquisition card PXI-5620, 14 bit resolution, 32 MHz sampling frequency, National Instrument®), transferred to a computer and analyzed by Labview® software.

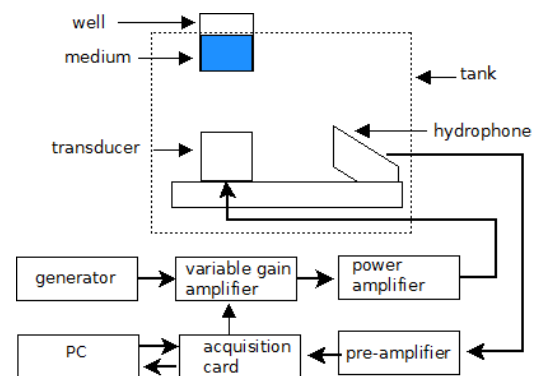


Figure 1: Experimental setup

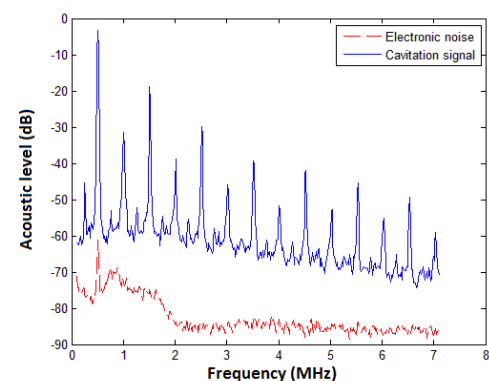


Figure 2: Example of instantaneous acoustic spectrum induced by a fixed intensity of 2.7 W/cm² and the reference noise which is subtracted to provide the inertial cavitation level.

The inertial cavitation level is determined by the subtraction of the non-referenced inertial cavitation level and the

reference noise. The non-referenced inertial cavitation level is defined as the average level of an instantaneous spectrum in dB within the range of 0.1 to 7.1 MHz. Before sonication, the reference noise is measured as the mean value of the inertial cavitation obtained when the excitation signal is off. An example of such spectra is shown in Figure 2.

2.2 Experimental results

Measurements of the inertial cavitation level are performed for increasing acoustic intensity and decreasing acoustic intensity for the same medium. The protocol of shots consists of successive ultrasonic excitations separated by times off. Each shot lasts 5 seconds and corresponds to a fixed acoustic intensity. When acoustic intensity increases, the inertial cavitation level sharply increases around the inertial cavitation threshold (Figure 3) around 2 W/cm². When acoustic intensity decreases, there is still inertial cavitation for acoustic intensities lower than the inertial acoustic threshold (for increasing intensities). The hysteresis effect is also observed for the harmonics and ultra-harmonics of the fundamental frequency. It is shown for the third harmonic of the fundamental frequency on Figure 4.

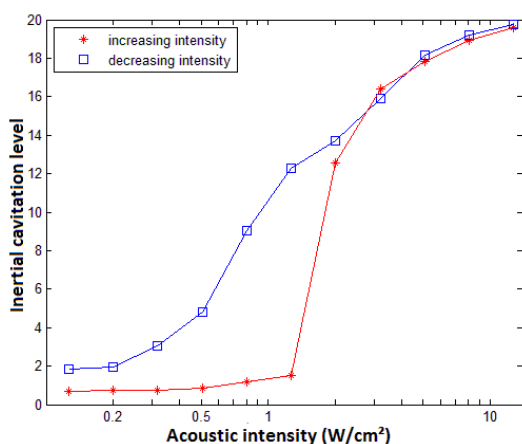


Figure 3: Example of experimental result for the inertial cavitation level evolution as a function of acoustic intensity, for increasing and decreasing intensity.

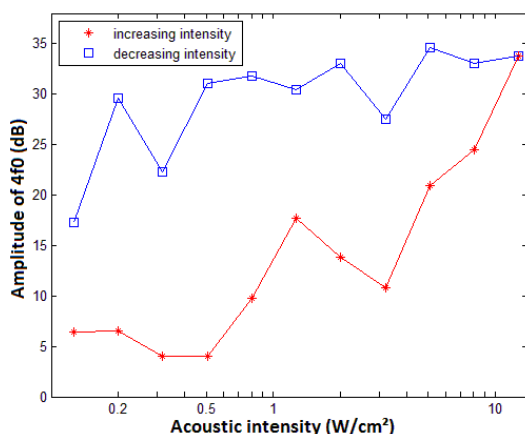


Figure 4: Example of experimental evolution of the third harmonic amplitude as a function of acoustic intensity, for increasing and decreasing intensity.

3 Numerical investigation

Figure 3 and 4 indicate a similar dependency with the applied acoustic intensity for both inertial cavitation and harmonics' amplitude, pointing out a hysteresis effect. This effect, observed simultaneously on the inertial cavitation level (and thus related to collapsing bubbles that experience after fragmentation) and harmonics' amplitude (related to bubble oscillation, rectified diffusion during the ultrasound shot), suggests that the cavitation activity is highly dependent on the evolution of the whole bubble distribution inside the medium. In the following, this hysteretic effect is studied numerically by investigating the modification of the bubble distribution during an ultrasound protocol similar to the experimental one.

3.1 Numerical model

According to the experimental results, bubbles in both stable and inertial cavitation play a role in the hysteretic effect. For chosen bubble radius and applied acoustic pressure, stable or inertial cavitation is expected, depending on the inertial cavitation threshold that spares these two cavitation regimes. This threshold is obtained by solving the Rayleigh-Plesset equation, assuming polytropic behavior of gas and neglecting thermal and acoustic dissipation [2]:

$$R\ddot{R} + \frac{3}{2}\dot{R}^2 + \frac{4\mu}{\rho R}\dot{R} = \frac{p_v(T_\infty) - [p_\infty - \delta p(t)]}{\rho} + \frac{p_g}{\rho} \left(\frac{R_0}{R}\right)^{3k}, \quad (1)$$

where p_∞ and T_∞ are the pressure and temperature far from the bubble, p_v is the vapor pressure, k the polytropic exponent, ρ and μ the liquid density and viscosity, p_g the gas pressure defined by $p_g = p_\infty - p_v(T_\infty) + 2S/R_0$ with S the surface tension. The cavitation threshold is defined as the intensity for which the bubble wall velocity exceeds the sound velocity in the surrounding liquid, effect which is generally identified as an indicator of inertial cavitation. This equation is computed for a sinusoidal acoustic perturbation $\delta p(t)$ at the experimental acoustic frequency and for pressures ranged between 0.1 to 100 bars. The evolution of the maximum velocity attained by the bubble wall is shown in Figure 5. Two regions of intensity clearly appear depending on the applied acoustic pressure: a linear / quasi-linear region for low pressure amplitudes separated from a strongly nonlinear region for higher amplitude by a sudden increase in the maximum velocity.

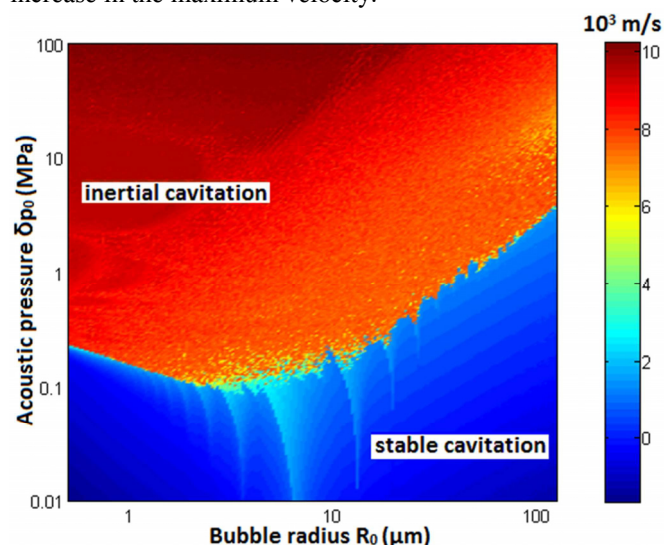


Figure 5: Evolution of the maximum velocity attained by the bubble for initial conditions $(R_0, \delta p_0)$. Initial bubble radius

ranges from 0.5 μm to 150 μm and acoustic pressure from 0.1 to 100 bars.

For a given acoustic pressure, a bubble depending of its initial radius, could be in the stable cavitation zone and so undergo rectified diffusion or be in the inertial cavitation zone and collapse and be fragmented in several daughter bubbles. During the time off between excitations, two mechanisms are applied on bubbles: dissolution and rising bubbles. These mechanisms are modelled and applied to bubble distributions. At the beginning, an initial bubble distribution for the medium before excitation is extrapolated from [7]. Bubble radius is ranged between 3 and 102 μm . For a chosen acoustic pressure, a chosen time of excitation and a chosen time off between two shots, the rectified diffusion or fragmentation is applied to the initial bubble distribution (Figure 6), depending on the status of bubbles according to the cavitation threshold. A new bubbles distribution is obtained. This process could be repeated several times during the acoustic excitation. At the end of the excitation time, a bubble distribution after excitation is found. Then, the time of dissolution is compared to the time off chosen. The distribution evolves by cancelling bubbles that need less than the time off to dissolve or to rise. Dissolution is applied to the remaining bubbles and a bubble distribution after time off is obtained. This third distribution becomes the initial distribution of another acoustic excitation for the next acoustic pressure. Numerical results presented later in sections 3.3 and 3.4 are obtained for 11 successive excitations, with increasing and decreasing acoustic intensity between 0.17 and 16.9 W/cm^2 , 1 loop of rectified diffusion / fragmentation, a 5 second time of excitation and a 0.1 second time off between 2 acoustic excitations.

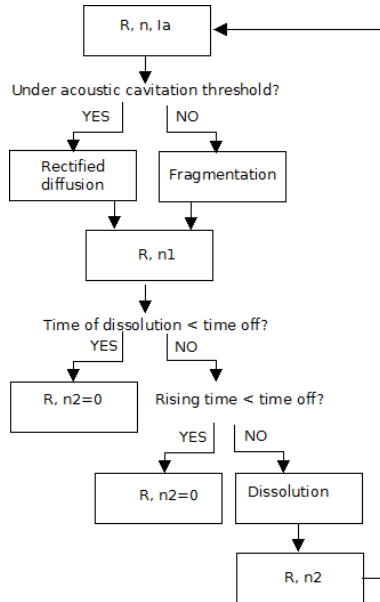


Figure 6: Organization chart of the programme.

3.2 Models of mechanisms

a. Rectified diffusion

During the acoustic excitation, dissolved gas in the medium are moved in the vicinity of bubbles thanks to the energy of the acoustical wave. There is a dissymmetry between gas diffusion inside the bubble during the expansion of the cavity and gas diffusion outside during the contraction of the cavity. The gas diffusion inside the bubble is more important than

the diffusion outside, so bubbles grow. There are different models of rectified diffusion on a single oscillating bubble in an acoustic field. We choose a model describing the evolution of the equilibrium radius [8]:

$$\frac{dR_0}{dt} = \frac{Dd_1}{R_0} \left[\left\langle \frac{R}{R_0} \right\rangle \left(1 + \frac{4\sigma}{3P_h R_0} \right)^{-1} \left(\frac{c_i}{c_s} - \frac{\left\langle \left(\frac{R}{R_0} \right)^4 (P_g/P_h) \right\rangle}{\left\langle \left(\frac{R}{R_0} \right)^4 \right\rangle} \right) \right], \quad (2)$$

where D is the gas diffusion coefficient, R_0 is the bubble radii at the equilibrium, σ is the surface tension, P_h is the hydrostatic pressure, c_i et c_s are respectively the initial and saturated dissolved gas concentration in the liquid. The parameter d_1 and all time average terms are given in [8].

b. Fragmentation

When a bubble moved above the inertial cavitation threshold, it collapses violently, sometimes in less than an acoustical period, in several smaller bubbles. The phenomenon of bubble fragmentation is still misunderstood, and the knowledge of the number of daughter bubbles is an open question [9,10,11]. Because the fragmentation is a random process, the number of daughter bubbles is determined as a random number ranged between 2 and 50.

c. Dissolution

When the acoustic excitation is turned off, bubbles begin to dissolve. They need to equilibrate their intern gas pressure with the term $2\sigma/R$ depending on the surface tension. The time of bubbles dissolution depends on the dissolved gas concentration in the medium, and is calculated with the Epstein-Plesset equation [12]:

$$\frac{dR}{dt} = \frac{c_s D}{\rho_g} \left(\frac{c_i}{c_s} - 1 - \frac{2\sigma}{R P_h} \right) \left(\frac{1}{R} + \frac{1}{\sqrt{\pi D t}} \right), \quad (3)$$

where, c_i et c_s are respectively the initial and saturated dissolved gas concentration in the liquid, D is the gas diffusion coefficient, g is the acceleration of gravity, ρ_g is the gas density, σ is the surface tension, P_h is the hydrostatic pressure and R is the instantaneous bubble radius.

d. Rising bubbles

At the beginning of the time off, bubbles are in equilibrium. Two main forces brought on the bubble are taken into account: the drag force, which is brought downward, and the buoyancy force, which is upward. To determine these forces and because the liquid studied is a low viscosity one, a simplified bubble model is chosen. The bubble is viewed as an empty non oscillating sphere and the drag force associated is written as [13]:

$$F_{drag} = -4\pi\mu Rv, \quad (4)$$

where μ , is the dynamic viscosity and v , the bubble velocity. The buoyancy force could be written as,

$$F_{buoyancy} = \frac{4\pi}{3} g(\rho_g - \rho_l) R^3, \quad (5)$$

where g is the acceleration of gravity, ρ_l and ρ_g are respectively the liquid and gas density and R is the instantaneous bubble radius.

When $F_{drag} < F_{buoyancy}$, bubble rise. For a given time off, bubbles with equilibrium radius greater than $R_{cri} = \sqrt{\frac{-3\mu h}{g(\rho_g - \rho_l)t_{off}}}$ are not present in the medium anymore.

For more accuracy and especially for bubbles whose radius is smaller than the critical radius, the dissolution phenomenon is taken into account in the rising time.

3.3 Bubble distribution evolution

The evolution of the inertial cavitation level depends on the evolution of bubble distribution in time. These distributions are observed for increasing and decreasing intensity and for chosen times off. We are expecting that the radius for which the number of bubbles is the most important is the resonant radius. This resonant radius is acoustic frequency (f) dependent and can be approximated in water by the Minneart equation, $R = 3/f$ [2]. We can see that when the intensity changes, the distribution of the collapsing bubbles stay around the same radius after a certain time (Figure 7) and is greater for the radius class containing the resonant radius, 6 μm . When the intensity increases, the number of bubbles increases too. At the same intensity, the distribution shape is quite the same when increasing or decreasing intensity, but the number of bubbles is greater while decreasing intensity, which suggests a more important inertial cavitation level.

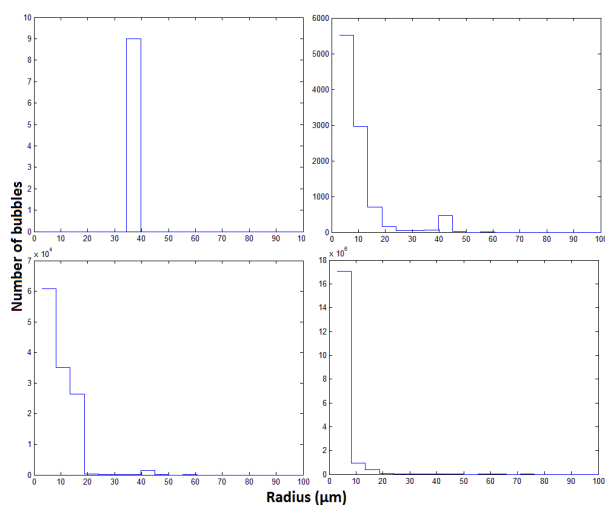


Figure 7: Distribution of collapsing bubbles for successive shots for increasing and decreasing acoustic intensity between 0.17 and 16.9 W/cm^2 , for a 5 second time of excitation, 1 loop of excitation and a 0.1 second time off. Upper left: 0.68 W/cm^2 (increasing intensity), upper right: 4.23 W/cm^2 (increasing intensity), lower left: 8.29 W/cm^2 (increasing intensity) and lower right: 4.23 W/cm^2 (decreasing intensity).

3.4 First approach of numerical cavitation index

The interpretation of the acoustic spectrum of a bubble cloud with bubbles interacting between them is still a hard challenge. In [14], numerical spectra of a bubble cloud composed of interacting monodisperse bubbles have been obtained using a modified Keller equation. This approach, using the quantification of the pressure of acoustic waves radiated from bubbles, could lead to the implementation of a numerical inertial cavitation index. As the distribution of all the collapsing bubbles is here taken into account, a first insight of a numerical inertial cavitation level is found as the energy of collapsing bubbles. This energy, according to [15] is proportional to the radiated energy of a single bubble:

$$E_{collapse} = 0.6 E_{bubble}, \quad (6)$$

with,

$$E_{bubble} = \frac{4\pi}{3} P_h R_{max}^3, \quad (7)$$

where p_∞ is the pressure far from the bubble, P_h is the hydrostatic pressure, R_{max} is the radius at which the bubble will collapse. For each radius above the inertial cavitation threshold curve, the numerical inertial cavitation level is chosen as:

$$IC_{numeric} = 0.6 \frac{\frac{4\pi}{3} P_h R^3}{\frac{4\pi}{3} P_h R_{min}^3} n, \quad (8)$$

where R is a radius of a bubble which collapse (a radius at which fragmentation is applied), n is the number of bubbles at the radius R and R_{min} is the smaller radius used in this numeric simulation. It is used to normalize the numerical inertial cavitation level. Figure 8 shows an example of the evolution of the numerical inertial cavitation level, in logarithmic scale, for increasing and decreasing acoustic intensity. The hysteresis effect is observed and presents qualitatively the same behaviour compared to experimental results. Especially, the sharp increase of cavitation level is found around the inertial cavitation threshold, with an increase in inertial cavitation events when decreasing the applied acoustic intensity. This hysteresis curve in decreasing intensity joins the one obtained for increasing intensity at the same cavitation threshold (around 0.5 W/cm^2) because of the definition of the inertial cavitation threshold curve presented in Figure 5.

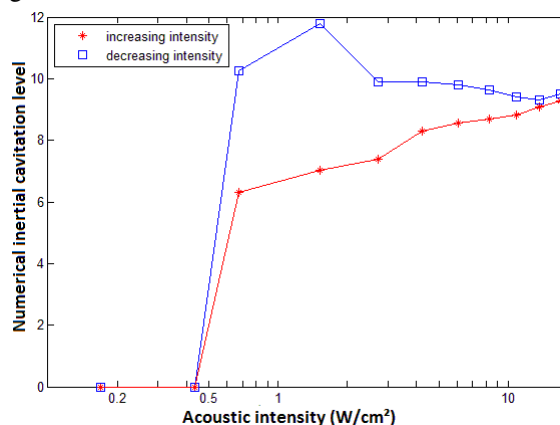


Figure 8: Example of result for the numerical inertial cavitation level as a function of acoustic intensity for increasing and decreasing intensity for a 5 second time of excitation, one loop of excitation and a 0.1 second time off.

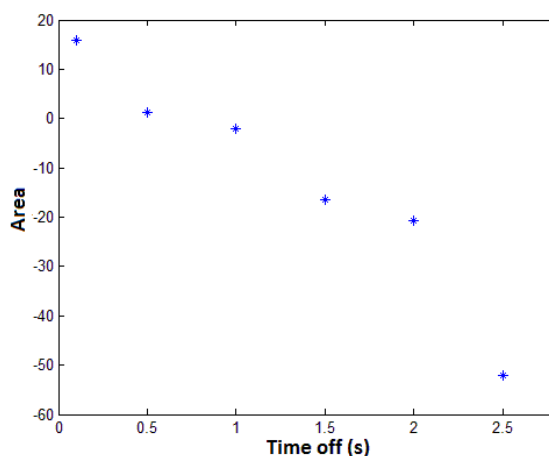


Figure 9: Evolution of the hysteresis area as a function of time off between excitations. It corresponds to 1 loop of excitation in the model and a 5 second time of excitation.

Considering the mechanisms involved in the hysteresis effect, particularly during time off (dissolution, rising of bubbles), the influence of time off between excitations is studied numerically by calculating the area of the hysteresis for different times off. An example of result is shown in Figure 9. Due to the possibility for more bubbles to disappear when increasing time off, the area of the hysteresis becomes smaller and even negative. The experimental validation of this result is currently in progress.

4 Conclusion

Measurements of the inertial cavitation level have been performed for increasing and decreasing intensity. A hysteresis effect has been found for the inertial cavitation level and the amplitude of harmonics and ultra-harmonics of the fundamental frequency versus the applied acoustic intensity. This effect is related to the evolution of the bubble distribution in the medium during the successive ultrasound irradiation when increasing and decreasing the acoustic intensity. The main mechanisms involved in the bubble distribution evolution have been numerically studied. These mechanisms are rectified diffusion and fragmentation during the acoustic excitation, and dissolution and rising bubble during the time off between two acoustic excitations. For an ultrasound protocol similar to the experimental one, bubble distribution evolves with a greater number of bubbles around the resonant radius. A first insight of the numerical inertial cavitation level was estimated as the energy of the collapsing bubbles for the whole bubble distribution. This numerical inertial cavitation level presents a hysteretic effect with a qualitative behaviour similar to the experimental results.

Acknowledgments

This work is supported by the French National Research Agency ANR project "SonInCaRe", n° 2010-TECS-003-01.

References

- [1] C. Coussios, R. Roy, "Applications of Acoustics and Cavitation to Noninvasive Therapy and Drug Delivery", *Annual Review of Fluid Mechanics* 40, 395-420 (2008)
- [2] T. G. Leighton, *The Acoustic Bubble*, Academic Pres, London, England (1994)
- [3] L. Reslan, J-L. Mestas, S. Herveaus, J-C. Béra, C. Dumontet, "Transfection of cells in suspension by ultrasound cavitation", *J. Control Release.* 142, 251-258 (2010)
- [4] D.M. Hallow, A.D. Mahajan, T.E. McCutchen, M.R. Prausnitz, "Measurement and correlation of acoustic cavitation with cellular bioeffects", *Ultrasound Med. Biol.* 32, 1111-1122 (2006)
- [5] A. Sabraoui, C. Insera, B. Gilles, J-C. Béra, J-L. Mestas, "Feedback loop process to control acoustic cavitation", *Ultrasonics Sonochemistry.* 18, 589-594 (2011)
- [6] J. Frohly, S. Labouret, C. Bruneel, I. Looten-Baquet, R. Torguet, "Ultrasonic cavitation monitoring by acoustic noise power measurement", *J. Acoust. Soc. Am.* 108(5), 2012-2020 (2000)
- [7] C. Brennen, *Cavitation and Bubble Dynamics*, New York: Oxford University Press, London (1995)
- [8] L.A. Crum, "Measurements of the growth of air bubbles by rectified diffusion", *J. Acoust. Soc. Am.* 68(1), 203-211 (1980)
- [9] C.C. Church, H.G. Flynn, "A mechanism for the generation of cavitation maxima by pulsed ultrasound", *J. Acoust. Soc. Am.* 76(2), 505-512 (1984)
- [10] V.A. Akulichev, "Inception and development of acoustic cavitation", *Akust. Inst. Acad. Nauk. SSSR, Moscow*, (1996)
- [11] W. Lauterborn, "Cavitation bubble dynamics-new tools for an intricate problem", *Applied Science Research* (1982)
- [12] P.S. Epstein, M.S. Plesset, "On the stability of gas bubble in liquid-gas solutions", *Journal of Chemical Physics*, (1950)
- [13] W. Lauterborn, T. Kurz, "Physics of bubble oscillations", *Reports on Progress in Physics*, 2010
- [14] K. Yasui, T. Tuziuti, J. Lee, T. Kuzuka, A. Towata, Y. Iida, "Numerical simulations of acoustic cavitation noise with the temporal fluctuation in the number of bubbles", *Ultrasonics Sonochemistry.* 17, 460-472 (2010)
- [15] A. Vogel, W. Lauterborn, "Acoustic transient generation by laser-produced cavitation bubbles near solid boundaries", *J. Acoust. Soc. Am.* 84(2), 719-731 (1988)